Stability analysis of boundary layer flow due to the presence of a small hole on a surface

R. Fernandez-Feria
Universidad de Malaga, E.T.S. Ingenieros Industriales, 29013 Malaga, Spain
(Received 23 October 2001; published 13 February 2002)

A linear, temporal, and viscous stability analysis of the boundary layer induced on a solid plane by a three-dimensional potential sink flow is considered. The flow is inviscidly (neutrally) stable. For axisymmetric perturbations, one can analyze separately the stability of those perturbations with a purely circumferential motion, and those with no azimuthal velocity. The first ones are shown to be always stable, a result that is found analytically. The second ones become unstable in a range of (high) Reynolds numbers that depends on the radial wave number. Finally, it is shown that all nonaxisymmetric perturbations are linearly stable.

DOI: 10.1103/PhysRevE.65.036307 PACS number(s): 47.20.−k, 47.15.−x

I. INTRODUCTION

The study of the hydrodynamic stability of the viscous boundary layer induced on a plane wall by a three-dimensional potential sink flow, whose velocity and pressure fields may be written in cylindrical polar coordinates (r,θ,z) as

$$(u,v,w)=\frac{Q}{4\pi(r^2+z^2)^{3/2}}(-r,0,-z), \tag{1a}$$

$$p=p_o-\frac{1}{2}\rho(u^2+w^2), \tag{1b}$$

($Q/2$ is the flow rate, p_o a reference pressure, and ρ the fluid density), is of interest for two reasons. First, because the stability properties of such a basic solution to the boundary layer equations (described in the next section), that models the boundary layer flow due to the presence of a small hole on a solid surface sufficiently away from the hole, are not known (to our knowledge). Shusser and Weihs [1] considered the inviscid stability of the potential sink (1a), finding that it is always inviscidly stable. However, no stability analysis of the viscous boundary layer induced by such a potential flow on the plane of the sink $z=0$ has been given. Known are the stability properties of the boundary layer induced by a two-dimensional sink flow (see, e.g., Ref. [2], pp. 231–233), but not of its three-dimensional counterpart.

The second reason, which has been the main motivation of the present work, is that the stability analysis of that model flow may shed some light on the problem of the self-generation of swirl in a sink flow. Well known is the fact that a vortex is sometimes formed superimposed to the flow through a hole (the so-called ''bathtub vortex''). Quantitative experiments in open [3] and closed [4] sink flows have shown that the vortex is formed above a critical Reynolds number based on the sink flow rate, suggesting that the phenomenon may be due to an instability of the sink flow. However, even if that is the case, which we do not know at present, since the three-dimensional viscous flow through a hole is a very complex flow, it is not an easy task to find out the nature of the hydrodynamic instability. For instance, we do not know in which part of the flow is the instability originated (if any), or whether it is a linear or a nonlinear instability, or whether it is an axisymmetric or a nonaxisymmetric instability. Recent works suggest that self-rotation is a nonaxisymmetric phenomenon (see, e.g., Ref. [5]). But, of the other two questions we have no clear idea. In the present work we try to delimit the regions of inquiry by analyzing the *linear* stability of a self-similar solution to the boundary layer equations that models, for high Reynolds numbers, the flow in the vicinity of the plane where the hole is located, provided that we are not in the immediate neighborhood of the hole. The self-similar solution that constitutes the basic flow of the stability analysis is given in the next section, together with the stability equations and a discussion of the numerical method used to solve them. Section III describes the stability results, both for axisymmetric and nonaxisymmetric perturbations. Finally, some conclusions are given in Sec. IV.

II. FORMULATION OF THE PROBLEM

A. Basic flow

For high Reynolds numbers (the precise Reynolds number will be defined below), the viscous flow originated by the interaction of the potential sink flow (1a), (1b) with a solid plane located at $z=0$ is governed, near the wall, by the following boundary layer equations and boundary conditions:

$$\frac{1}{r}\frac{\partial ru}{\partial r}+\frac{\partial w}{\partial z}=0, \tag{2}$$

$$u\frac{\partial u}{\partial r}+w\frac{\partial u}{\partial z}=-\frac{Q^2}{8\pi^2r^5}+\nu\frac{\partial^2u}{\partial z^2}, \tag{3}$$

$$u=w=0 \quad \text{at} \quad z=0, \tag{4}$$

$$u\to-\frac{Q}{4\pi r^2} \quad \text{as} \quad z/\delta(r)\to\infty, \tag{5}$$

where ν is the kinematic viscosity, and the boundary layer thickness $\delta(r)$ is defined below. This problem has a self-similar solution, first described by Mangler (using spherical rather than cylindrical coordinates; see, e.g., Ref. [6], p. 428). In fact, defining

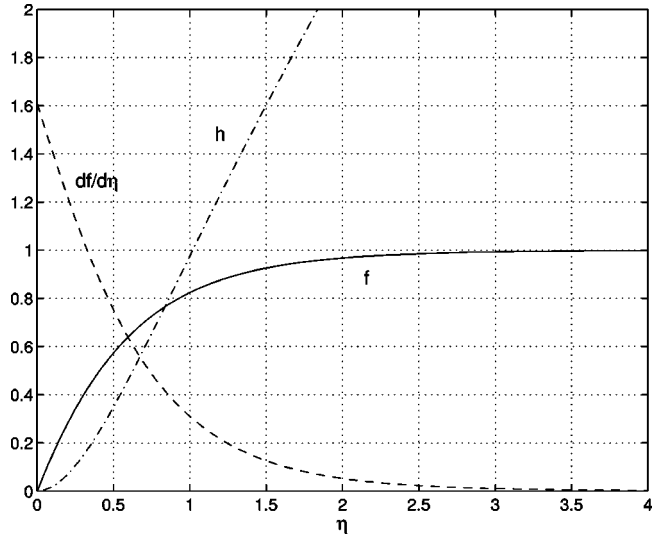

FIG. 1. Self-Similar solution for the basic flow.

$$u=-\frac{Q}{4\pi}\frac{f(\eta)}{r^2},\quad w=-\sqrt{\frac{Q\nu}{4\pi}}\frac{h(\eta)}{r^{3/2}}, \tag{6}$$

$$\eta=\frac{z}{\delta(r)},\quad \delta(r)=\frac{r^{3/2}}{\sqrt{\frac{Q}{4\pi\nu}}}, \tag{7}$$

Eqs. (2)–(5) become

$$f+\frac{3}{2}\eta f'-h'=0, \tag{8}$$

$$f''+2+hf'-f\left(2f+\frac{3}{2}\eta f'\right)=0, \tag{9}$$

$$f(0)=h(0)=0,\quad f(\infty)=1, \tag{10}$$

where the primes mean differentiation with respect to η. Equations (8) and (9) may be reduced further to a single, third-order differential equation if one uses the self-similar form of the stream function instead of f and h. In that form, the resulting equation was first integrated numerically by Terrill [7]. The numerical solution shown in Fig. 1 is obtained directly from Eqs. (8)–(10) using a standard finite difference method with deferred corrections.

It is convenient to define the *local* Reynolds number

$$R=\frac{r}{\delta(r)}=\sqrt{\frac{Q}{4\pi\nu r}}. \tag{11}$$

One can also define a Reynolds number based on the local displacement thickness of the boundary layer,

$$\delta_1(r)=\int_0^\infty\left(1-\frac{u}{U_o}\right)dz=\delta(r)\int_0^\infty[1-f(\eta)]d\eta$$
$$\simeq 0.585\,397\delta(r), \tag{12}$$

where $U_o=Q/(4\pi r^2)$. Thus,

$$R_1=\frac{\delta_1 U_o}{\nu}\simeq 0.585\,397R. \tag{13}$$

Comparing Eq. (1a) with Eq. (5), it is clear that the above self-similar solution is valid for $z\ll r$, so that it is not valid, obviously, in the close vicinity of the sink ($r=0$). In terms of the self-similar variable and the local Reynolds number, this condition can be written

$$\eta\ll R. \tag{14}$$

From Fig. 1, this means that R must be *much larger* than approximately 4.

B. Stability equations

To analyze the linear stability of the above base flow, the flow variables (u,v,w) and p are decomposed, as usual, into the mean part, Eqs. (6) and (1b), and small perturbations:

$$u=\frac{Q}{4\pi r^2}[-f(\eta)+\overline{u}], \tag{15}$$

$$v=\frac{Q}{4\pi r^2}\overline{v}, \tag{16}$$

$$w=\frac{Q}{4\pi r^2}\left(-\frac{h(\eta)}{R}+\overline{w}\right), \tag{17}$$

$$\frac{p-p_o}{\rho}=\frac{1}{2}\left(\frac{Q}{4\pi r^2}\right)^2(-1+\overline{p}). \tag{18}$$

The dimensionless independent variables (R,θ,η) will be used instead of (r,θ,z). Making use of the near-parallel flow approximation $(R\gg 1)$, the dimensionless perturbations

$$\mathbf{s}\equiv[\overline{u},\overline{v},\overline{w},\overline{p}]^T, \tag{19}$$

are decomposed in the standard form

$$\mathbf{s}=\mathbf{S}(\eta)e^{iR(-\alpha+n\theta-\omega\tau)}. \tag{20}$$

In this expression,

$$\mathbf{S}(y)\equiv\begin{pmatrix}F(\eta)\\G(\eta)\\H(\eta)\\\Pi(\eta)\end{pmatrix}, \tag{21}$$

is the (complex) amplitude of the perturbations,

$$\tau=\frac{Q}{4\pi r^3}t, \tag{22}$$

is the dimensionless time, and

$$\alpha=\hat{\alpha}\delta(r), \quad n=\frac{\hat{n}}{R}, \quad \omega=\frac{4\pi r^3}{Q}\frac{\hat{\omega}}{R}, \tag{23}$$

are the local, order of unity, dimensionless radial wave number, azimuthal wave number, and frequency, respectively ($\hat{\alpha}$ and $\hat{\omega}$ are the dimensional radial wave number and frequency, respectively).

Substituting Eqs. (15)–(23) into the incompressible Navier-Stokes equations, neglecting terms $O(R^{-2})$, in accordance with the boundary layer approximation, and second-order terms in the small perturbations, one obtains the following linear stability equation:

$$\mathbf{L}\cdot\mathbf{S}=i\omega\mathbf{L}_0\cdot\mathbf{S}, \tag{24}$$

where

$$\mathbf{L}_0=\begin{pmatrix}0&0&0&0\\1&0&0&0\\0&1&0&0\\0&0&1&0\end{pmatrix}, \tag{25}$$

$$\mathbf{L}\equiv\mathbf{L}_1+i\alpha\mathbf{L}_2+\frac{1}{R}\mathbf{L}_3+\frac{\alpha^2}{R}\mathbf{L}_0, \tag{26}$$

$$\mathbf{L}_1=\begin{pmatrix}0&in&\frac{d}{d\eta}&0\\0&0&-\frac{df}{d\eta}&0\\0&0&0&\frac{in}{2}\\0&0&0&\frac{1}{2}\frac{d}{d\eta}\end{pmatrix}, \tag{27}$$

$$\mathbf{L}_2=\begin{pmatrix}-1&0&0&0\\f&0&0&-\frac{1}{2}\\0&f&0&0\\0&0&f&0\end{pmatrix}, \tag{28}$$

$$\mathbf{L}_3=\begin{pmatrix}-1-\frac{3}{2}\eta\frac{d}{d\eta}&0&0&0\\4f+\frac{3}{2}\eta\frac{df}{d\eta}+n^2+D_\eta&0&0&-2-\frac{3}{4}\eta\frac{d}{d\eta}\\0&f+n^2+D_\eta&0&0\\0&0&2f-\frac{dh}{d\eta}+n^2+D_\eta&0\end{pmatrix}, \tag{29}$$

$$D_\eta=\frac{3}{2}\eta f\frac{d}{d\eta}-h\frac{d}{d\eta}-\frac{d^2}{d\eta^2}. \tag{30}$$

This equation has to be solved with the following boundary conditions:

$$F(0)=G(0)=H(0)=0, \tag{31}$$

$$F(\infty)=G(\infty)=H(\infty)=0. \tag{32}$$

In the temporal stability analysis that will be carried out here, for a given *real* radial wave number α, and given the parameters R and n, the system (24)–(32) constitutes a linear eigenvalue problem for the complex frequency

$$\omega=\omega_r+i\omega_i. \tag{33}$$

The flow is considered unstable when $\omega_i>0$. Since we are interested in perturbations approaching the sink (i.e., the evolution of perturbations for decreasing values r, which, according to Eq. (11), corresponds to increasing values of R), only positive values of α will be considered. Also, since the mean flow has no circumferential motion, positive and negative values of the azimuthal wave number n will yield the same results, so that only positive values of n will be considered.

C. Numerical method

To solve Eqs. (24)–(32) numerically, the eigenfunction vector **S** is discretized using a staggered Chebyshev spectral collocation technique developed by Khorrami [8], where the three velocity components and the three momentum equations are discretized at the grid collocation points, whereas the pressure and the continuity equation are enforced at the mid grid points. This method has the advantage of eliminating the need of two artificial pressure boundary conditions, which are not included in Eqs. (31), (32). To implement the spectral numerical method, Eq. (24) is discretized by expanding **S** in terms of a truncated Chebyshev series. To map

the interval $0 \leqslant \eta < \infty$ into the Chebyshev polynomials domain $-1 \leqslant s \leqslant 1$, the transformation $\eta = c_1(1+s)/(c_2-s)$ is used, where c_1 is a constant ($c_1 = 3$ in all the computations) and $c_2 = 1 + 2c_1/\eta_{max}$. The boundary condition (32) is applied at $\eta = \eta_{max}$, which is chosen large enough to ensure that the results do not depend on that truncated distance. This transformation concentrates the Chebyshev collocation points near the plane $\eta = 0$, in such a way that approximately half of the points are located in the interval $0 \leqslant \eta \leqslant c_1$.

The domain is thus discretized in N points, N being the number of Chebyshev polynomials in which **S** has been expanded. For most of the computations reported below, values of N between 40 and 50 were enough to obtain the eigenvalues with at least 6 or 7 significant figures, as it was checked out for every result given below by using larger values of N. With this discretization (24)–(32) becomes an algebraic linear eigenvalue problem that is solved with double precision using an eigenvalue solver from the IMSL library (subroutine DGVCCG), which provides the entire eigenvalue and eigenvector spectrum. Spurious eigenvalues were discarded by comparing the computed spectra for increasing number N of collocation points.

III. RESULTS

From an inviscid point of view, the flow is stable according to Rayleigh's criterion, for the velocity profile $f(\eta)$ has no inflexion point. This is corroborated numerically by solving the stability equation in the formal limit $R \to \infty$ for any value of n. Actually, the flow is neutrally stable in this limit $R \to \infty$.

The viscous results (R large, but finite) will be presented for axisymmetric and nonaxisymmetric perturbations separately.

A. Axisymmetric perturbations

Since the base flow has no circumferential velocity component, axisymmetric perturbations ($n = 0$) may be classified within two different kinds: those with no azimuthal velocity component ($G \equiv 0, F \neq 0, H \neq 0, \Pi \neq 0$), which will be referred to as type *a* for short, and perturbations with only azimuthal motion ($F \equiv H \equiv \Pi \equiv 0, G \neq 0$), referred to as type *b*. Typical eigenfunctions belonging to each one of these two types of perturbations are plotted in Fig. 2, where $f(\eta)$ is also plotted as a reference. Note that the eigenfunction G for perturbations of type *b* is much more concentrated near the plane $\eta = 0$ than the eigenfunctions F and H in perturbations of type *a*. Results for perturbations of type *b* will be given first because they are easier to analyze, and because a general result on their stability can be obtained analytically.

1. Purely azimuthal perturbations

As indicated above, for $n = 0$, there exists a class of solutions to Eqs. (24)–(32) that are characterized by $F = H = \Pi = 0$. The remaining, nonvanishing component G of the amplitude of the perturbations satisfy the following eigenvalue problem:

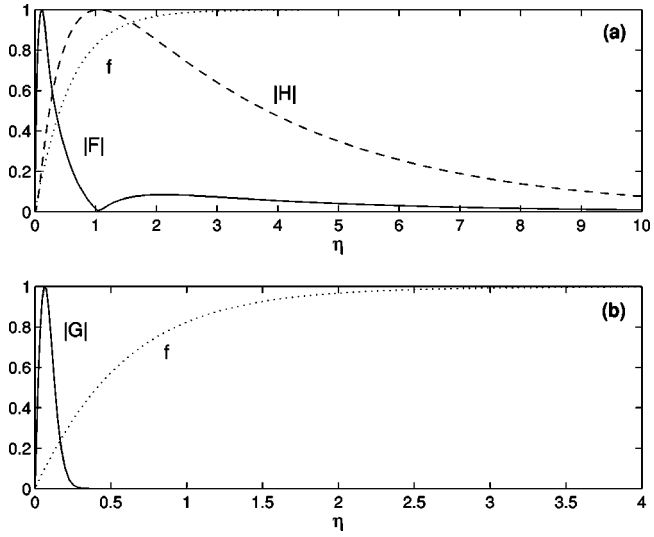

FIG. 2. Eigenfunctions corresponding to the less stable axisymmetric ($n = 0$) perturbations of type *a* (a), and type *b* (b), for $R = 43\,221$ and $\alpha = 0.3070$. The corresponding eigenvalues are $\omega_r = 5.477\,595\,81 \times 10^{-2}$, $\omega_i \simeq 0$, and $\omega_r = 3.544\,265\,53 \times 10^{-2}$, $\omega_i = -1.976\,272\,11 \times 10^{-2}$, respectively. The maximum value of all the eigenfunction components are normalized to unity. Also shown as a reference is $f(\eta)$.

$$\left[i\alpha f + \frac{1}{R}\left(f + \frac{3}{2}\eta f \frac{d}{d\eta} - h\frac{d}{d\eta} + \alpha^2 - \frac{d^2}{d\eta^2} \right) \right] G = i\omega G, \tag{34}$$

$$G(0) = G(\infty) = 0. \tag{35}$$

Using the standard transformation $G = g \exp[-\frac{1}{2}\int (h - \frac{3}{2}\eta f) d\eta]$, and defining

$$a = \alpha R, \quad \varpi = \omega R = \varpi_r + i\varpi_i, \tag{36}$$

Eqs. (34)–(35) can be written

$$g'' - \left[\frac{3}{4}f + \frac{1}{4}\left(h - \frac{3}{2}\eta f \right)^2 + i(af - \varpi) + \frac{a^2}{R^2} \right] g = 0, \tag{37}$$

$$g(0) = g(\infty) = 0, \tag{38}$$

where the primes denote differentiation with respect to η. Multiplying this equation by the complex conjugate g^*, integrating between $\eta = 0$ and $\eta = \infty$, integrating by parts, and using the boundary conditions, one obtains the following relations for the imaginary and real parts of the resulting expression:

$$\int_0^\infty (af - \varpi_r)|g|^2 d\eta = 0, \tag{39}$$

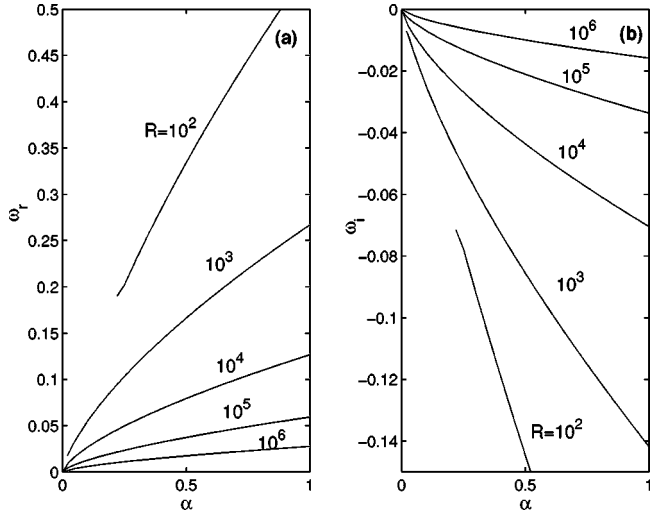

FIG. 3. Real (a) and imaginary (b) parts of ω as functions of α of the less stable axisymmetric perturbations of type *b* for several Reynolds numbers. All the curves $\omega_r(\alpha)$ collapse when plotted in the form $\varpi_r(a)$.

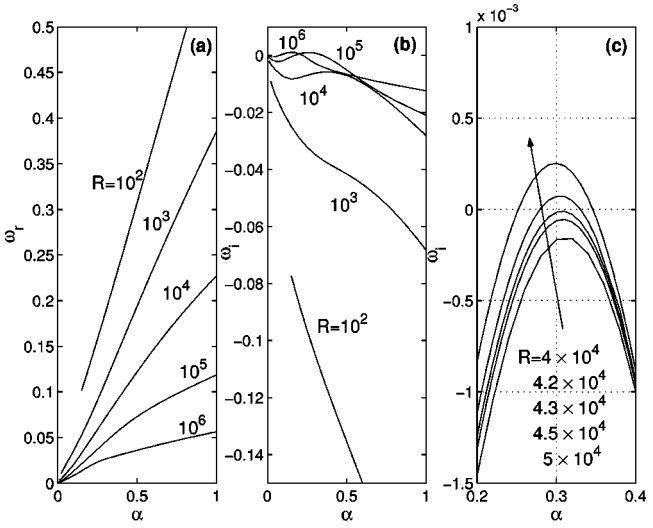

FIG. 4. Real (a) and imaginary (b) parts of ω as functions of α of the less stable axisymmetric perturbations of type *a* for several Reynolds numbers. (c) Detail of the functions $\omega_i(\alpha)$ near the critical values of α and R.

$$\varpi_i \int_0^\infty |g|^2 d\eta = -\int_0^\infty \left\{ \left|\frac{dg}{d\eta}\right|^2 + |g|^2 \left[\frac{3}{4} f + \frac{1}{4}\left(h - \frac{3}{2}\eta f \right)^2 + \frac{a^2}{R^2} \right] \right\} d\eta. \tag{40}$$

The first relation (39) tells us that the real part of the dispersion relation does not depend on the local Reynolds number R when written in the new variables (36), i.e., $\varpi_r(a)$. More important is the second relation (40), which says that these purely azimuthal perturbations are always stable, $\varpi_i \leqslant 0$, for every value of a and R, with the imaginary part of the dispersion relation, $\varpi_i(a)$, depending slightly on R for large R. All these results are corroborated numerically. Figure 3 shows the dispersion relation $\omega_r(\alpha)+i\omega_i(\alpha)$ of the less stable perturbations (largest ω_i) for several values of R. Note that $\omega_i<0$, and that the flow is increasingly more stable, for these purely azimuthal perturbations, as R decreases.

2. Meridional perturbations

For axisymmetric perturbations with no azimuthal velocity (perturbations of type a), there is no general criterion of stability, and the results have to be obtained numerically. As a fundamental difference with the azimuthal perturbations, it is found that perturbations of type *a* may be unstable in some ranges of the wave number α and the Reynolds number R. Figure 4 shows the dispersion relations $\omega(\alpha)$ for several Reynolds numbers. It is observed that the flow is unstable for high Reynolds numbers in a range of wave numbers α that depends on R (remember that the flow is neutrally stable for $R\to\infty$), and becomes stable for $R<R_c\simeq 43\,221$. This is better depicted in Fig. 5, where the neutral curves of stability on the (α,R) and the (ω_r,R) planes are plotted. The critical Reynolds number R_c corresponds to $\alpha_c\simeq 0.3070$ and $\omega_{rc}\simeq 5.4776\times 10^{-2}$ [see Fig. 2(a) for the eigenfunction]. In terms of the local displacement thickness of the boundary layer (12), the critical Reynolds number and critical wave number are $R_{1c}\simeq 25\,301$ and $\alpha_{1c}=\hat{\alpha}_c\delta_1=0.585\,397$ $\alpha_c\simeq 0.1797$. These values can be compared with those corresponding to a two-dimensional flow in the boundary layer along an infinite plane wall due to a line sink at the origin (see, e.g., Ref. [2], p. 233): $R_{1c}=21675$, $\alpha_{1c}=0.1738$.

It is observed in Fig. 4 (also in Fig. 3) that no results are given for $R=100$ when the wave number α is small. The reason is that, as αR decreases, the eigenfunctions become more extended in space, reaching higher values of η. Eventually, the eigenfunctions are different from zero at such a high value of η that the boundary layer approximation of the basic flow is no longer valid there. In particular, the computations show that for $\alpha R\leqslant 15$, approximately, the condition

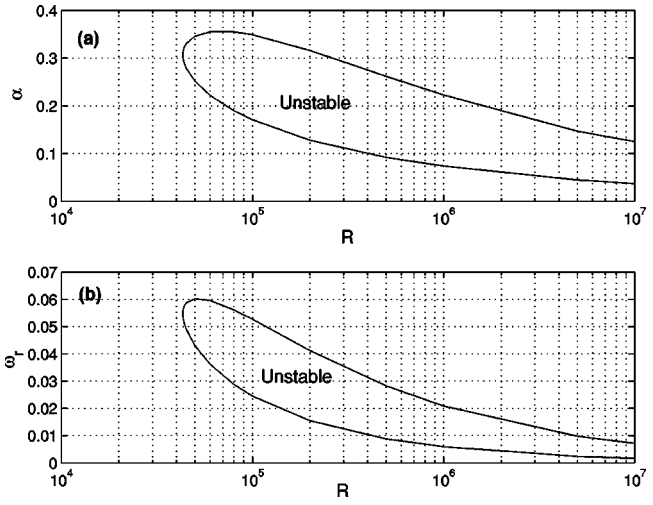

FIG. 5. Curves of marginal stability for axisymmetric perturbations of type *a* on the (α,R) plane, (a), and on the (ω_r,R) plane, (b).

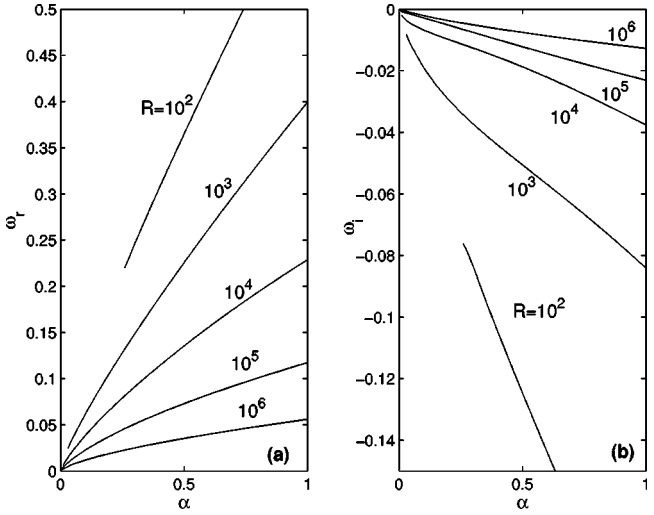

FIG. 6. Real (a) and imaginary (b) parts of ω as functions of α of the less stable nonaxisymmetric perturbations with $n=1$ for several Reynolds numbers.

(14) is not satisfied. Therefore, no results for $\alpha R \leqslant 15$, approximately, are given here.

B. Nonaxisymmetric perturbations

For local azimuthal wave number $n \neq 0$, all the eigenfunction components are always different from zero; i.e., all the eigenfunctions have azimuthal velocity component $G \neq 0$, as well as nonvanishing meridional components F and H. Numerically, the stability results are intermediate between those for type *a* and type *b* axisymmetric perturbations, but nearer to type *b*. In particular, it is found that, for $n=1$, the flow is stable for all Reynolds numbers (see Fig. 6). As n increases, the flow becomes more stable, particularly as R decreases. This can be observed in Figs. 7 and 8, where the dispersion relations for nonaxisymmetric perturbations with $n=1$ and $n=10$, together with the dispersion relations for axisymmetric perturbations of types *a* and *b*, are plotted for two different Reynolds numbers. For the highest value of R considered in these figures ($R=10^5$, Fig. 8), the results for nonaxisymmetric perturbations with $n=10$ approach those for type-*b* axisymmetric perturbations.

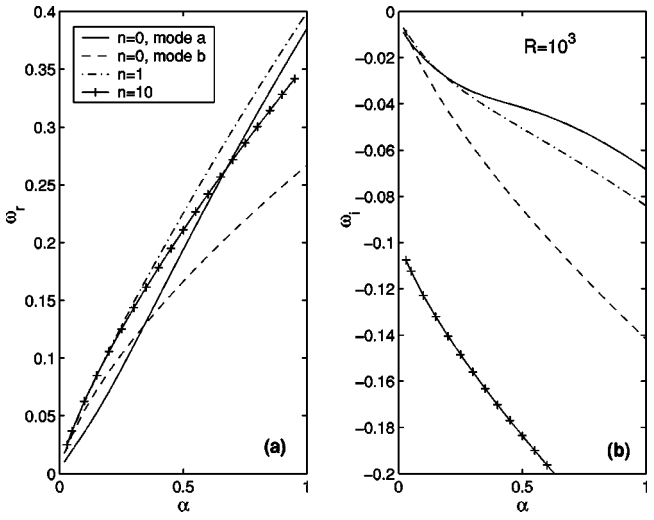

FIG. 7. Comparison between the real (a) and imaginary (b) parts of $\omega(\alpha)$ for the less stable axisymmetric perturbations ($n=0$) of types *a* and *b*, and nonaxisymmetric perturbations with $n=1$ and $n=10$, $R=10^3$.

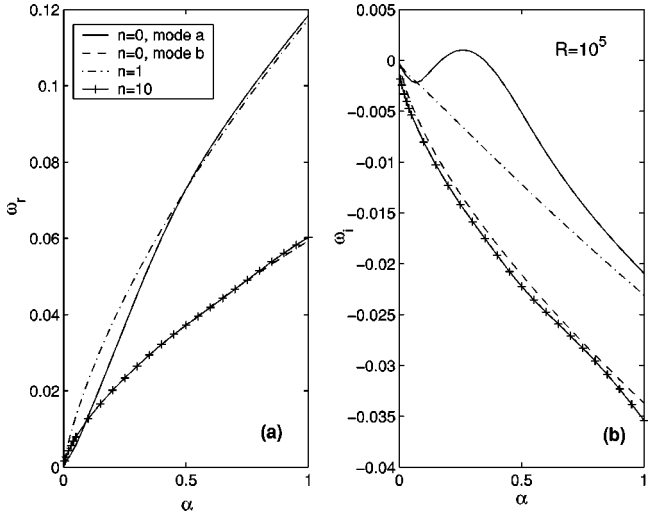

FIG. 8. As in Fig. 7, but for $R=10^5$.

IV. CONCLUSIONS

The stability analysis of the boundary layer flow due to the presence of a small hole on a surface performed in this paper has shown that the flow is unstable only for axisymmetric perturbations with no azimuthal velocity component. In particular, it is shown that the flow becomes unstable for local Reynolds numbers R larger than $R_c \simeq 43\,221$. This *viscous* instability (the flow is neutrally stable in the limit $R \rightarrow \infty$) is similar to that found for the two-dimensional version of this flow, namely, the boundary layer flow due to the presence of a two-dimensional (line) sink on a plane surface. The instability appears at a relatively high Reynolds number, marking the onset of turbulence. It has nothing to do with the formation of a vortex in the sink, a phenomenon that is shown experimentally to occur at much lower Reynolds numbers (e.g., Refs. [3,4]). Actually, this is quite clear from the fact that any perturbation containing an azimuthal velocity component is always stable. Thus, it is shown analytically [Eq. (40)] that axisymmetric perturbations with only azimuthal motion (called of *type b* in Sec. III) are always stable. On the other hand, nonaxisymmetric perturbations, which always contain an azimuthal velocity component, are also stable for all values on the azimuthal wave number n. In fact, their stability increase with n. Therefore, although the present results do not discard, of course, the instability origin of the vortex formation in a sink, they eliminate some possibilities. Thus, if the vortex formation is the consequence of an instability, either it does not come from the viscous boundary layer on the solid wall adjacent to, but not in the immediate neighborhood of, the hole, or, if it is a boundary-layer instability, it has to be a nonlinear instability. Another possibility that the present results do not discard is the phe-

nomenon caused by a near-wall instability, but occurring at such low Reynolds numbers and low wave numbers (i.e., at such a low value of αR) that the present boundary layer analysis cannot be used to find it out because the boundary layer approximation fails. In contrast to the present simple stability analysis, the investigation of any of these possibilities would require a full three-dimensional numerical simulation of the sink flow.

ACKNOWLEDGMENT

This research was supported by the Ministerio de Ciencia y Tecnología of Spain (Grant No. BFM00-1323).

[1] M. Shusser and D. Weihs, Phys. Fluids **7**, 2345 (1995).
[2] P.G. Drazin and W.H. Reid, *Hydrodynamic Stability* (Cambridge University Press, Cambridge, England, 1981).
[3] T. Kawakubo, Y. Tsuchiya, M. Sugaya, and K. Matsumura, Phys. Lett. **68A**, 65 (1978).
[4] R. Fernandez-Feria and E. Sanmiguel-Rojas, Phys. Fluids **12**, 3082 (2000).
[5] V. Shtern and F. Hussain, Annu. Rev. Fluid Mech. **31**, 537 (1999).
[6] *Laminar Boundary Layers*, edited by L. Rosenhead (Dover, New York, 1988).
[7] R.M. Terrill, Philos. Trans. R. Soc. London, Ser. A **253**, 55 (1960).
[8] M.R. Khorrami, Int. J. Numer. Methods Fluids **12**, 825 (1991).